Potential Modulated Multilayer Deposition of Multisegment Cu/Ni Nanowires with Tunable Magnetic Properties

Min Chen,† Chia-Ling Chien,‡ and Peter C. Searson*,†

Department of Materials Science and Engineering, and Department of Physics and Astronomy, Johns Hopkins University, Baltimore, Maryland 21218

Received October 12, 2005. Revised Manuscript Received December 2, 2005

Potential modulated multilayer deposition has been used to fabricate a series of multisegment Cu/Ni nanowires with diameters in the range of 40−140 nm. We show how the composition and microstructure are dependent on the deposition potential. The aspect ratio of the ferromagnetic nickel segments was varied from 0.1 (disk-shaped) to 2.5 (rod-shaped). The coercivity and remanence of the nanowires are strongly dependent on the diameter and aspect ratio as well as on dipolar coupling between the ferromagnetic segments. Micromagnetic simulations were used to model the magnetization hysteresis loops. These results show how potential modulated multilayer deposition can be used to tailor the properties of ferromagnetic particles.

Introduction

The magnetic behavior of nanoscale ferromagnetic objects is strongly dependent on both size and shape. Asymmetric particles, such as nanowires and nanorods, exhibit unique magnetic properties as a result of their inherent shape anisotropy.[1−4] For example, a magnetized ferromagnetic nanowire usually has an easy axis parallel to the wire axis and, in a suspension, will align parallel to an external magnetic field.[5]

Electrochemical template synthesis is a versatile technique for producing single component and multisegment nanowires and nanorods.[6,7] Ferromagnetic nanowires of metals such as Fe,[3,8,9] Co,[4,10,11] and Ni,[4,12,13] as well as ferromagnetic alloys such as CoPt,[14,15] FePt,[16] and FeCo,[17] have been fabricated using this technique. In some cases, multilayer nanowires of two components can be electrodeposited from the same solution. Systems that have been studied include Co/Cu,[18−20] Ni/Cu,[21,22] CoNi/Cu,[20,23] NiFe/Cu,[24−26] and Ag/Au.[27,28]

The magnetic properties of single component nanowires are dependent on the diameter and composition. Ferromagnetic nanowires generally exhibit very large coercivity and remanence along the magnetic easy axis, parallel to the wire axis, due to the inherent shape anisotropy and reduced dimensions.[1] The coercivity and remanence are dependent on the nanowire diameter and hence can be tuned by selection of the appropriate nanowire dimensions. The Curie temperature decreases with decreasing nanowire diameter and hence can be used to tailor the magnetic response.[13]

* To whom correspondence should be addressed. E-mail: searson@jhu.edu.
† Department of Materials Science and Engineering.
‡ Department of Physics and Astronomy.

(1) Ross, C. A.; Hwang, M.; Shima, M.; Cheng, J. Y.; Farhoud, M.; Savas, T. A.; Smith, H. I.; Schwarzacher, W.; Ross, F. M.; Redjdal, M.; Humphrey, F. B. *Phys. Rev. B* **2002**, *65*, 144417.
(2) Meier, J.; Doudin, B.; Ansermet, J. P. *J. Appl. Phys.* **1996**, *79*, 6010−6012.
(3) Sellmyer, D. J.; Zheng, M.; Skomski, R. *J. Phys.: Condens. Matter* **2001**, *13*, R433−R460.
(4) Whitney, T. M.; Jiang, J. S.; Searson, P. C.; Chien, C. L. *Science* **1993**, *261*, 1316−1319.
(5) Tanase, M.; Bauer, L. A.; Hultgren, A.; Silevitch, D. M.; Sun, L.; Reich, D. H.; Searson, P. C.; Meyer, G. J. *Nano Lett.* **2001**, *1*, 155−158.
(6) Possin, G. E. *Rev. Sci. Instrum.* **1970**, *41*, 772−774.
(7) Martin, C. R. *Science* **1994**, *266*, 1961−1966.
(8) Al Mawlawi, D.; Coombs, N.; Moskovits, M. *J. Appl. Phys.* **1991**, *70*, 4421−4425.
(9) Li, C. Z.; Lodder, J. C. *J. Magn. Magn. Mater.* **1990**, *88*, 236−246.
(10) Beeli, C.; Doudin, B.; Ansermet, J. P.; Stadelmann, P. *J. Magn. Magn. Mater.* **1996**, *164*, 77−90.
(11) Ferre, R.; Ounadjela, K.; George, J. M.; Piraux, L.; Dubois, S. *Phys. Rev. B* **1997**, *56*, 14066−14075.
(12) Sun, L.; Searson, P. C.; Chien, C. L. *Appl. Phys. Lett.* **1999**, *74*, 2803−2805.
(13) Sun, L.; Searson, P. C.; Chien, C. L. *Phys. Rev. B* **2000**, *61*, R6463−R6466.
(14) Mallet, J.; Yu-Zhang, K.; Chien, C. L.; Eagleton, T. S.; Searson, P. C. *Appl. Phys. Lett.* **2004**, *84*, 3900−3902.
(15) Huang, Y. H.; Okumura, H.; Hadjipanayis, G. C.; Weller, D. *J. Appl. Phys.* **2002**, *91*, 6869−6871.
(16) Chu, S. Z.; Inoue, S.; Wada, K.; Kanke, Y.; Kurashima, K. *J. Electrochem. Soc.* **2005**, *152*, C42−C47.
(17) Qin, D. H.; Cao, L.; Sun, Q. Y.; Huang, Y.; Li, H. L. *Chem. Phys. Lett.* **2002**, *358*, 484−488.
(18) Piraux, L.; George, J. M.; Despres, J. F.; Leroy, C.; Ferain, E.; Legras, R.; Ounadjela, K.; Fert, A. *Appl. Phys. Lett.* **1994**, *65*, 2484−2486.
(19) Liu, K.; Nagodawithana, K.; Searson, P. C.; Chien, C. L. *Phys. Rev. B* **1995**, *51*, 7381−7384.
(20) Blondel, A.; Meier, J.; Doudin, B.; Ansermet, J. P.; Attenborough, K.; Evans, P.; Hart, R.; Nabiyouni, G.; Schwarzacher, W. *J. Magn. Magn. Mater.* **1995**, *148*, 317−318.
(21) Chen, M.; Sun, L.; Bonevich, J. E.; Reich, D. H.; Chien, C. L.; Searson, P. C. *Appl.Phys. Lett.* **2003**, *82*, 3310−3312.
(22) Wang, L.; YuZhang, K.; Metrot, A.; Bonhomme, P.; Troyon, M. *Thin Solid Films* **1996**, *288*, 86−89.
(23) Evans, P. R.; Yi, G.; Schwarzacher, W. *Appl. Phys. Lett.* **2000**, *76*, 481−483.
(24) Dubois, S.; Marchal, C.; Beuken, J. M.; Piraux, L.; Duvail, J. L.; Fert, A.; George, J. M.; Maurice, J. L. *Appl. Phys. Lett.* **1997**, *70*, 396−398.
(25) Dubois, S.; Piraux, L.; George, J. M.; Ounadjela, K.; Duvail, J. L.; Fert, A. *Phys. Rev. B* **1999**, *60*, 477−484.
(26) Maurice, J. L.; Imhoff, D.; Etienne, P.; Durand, O.; Dubois, S.; Piraux, L.; George, J. M.; Galtier, P.; Fert, A. *J. Magn. Magn. Mater.* **1998**, *184*, 1−18.
(27) Nicewarner-Pena, S. R.; Freeman, R. G.; Reiss, B. D.; He, L.; Pena, D. J.; Walton, I. D.; Cromer, R.; Keating, C. D.; Natan, M. J. *Science* **2001**, *294*, 137−141.
(28) Ji, C. X.; Oskam, G.; Ding, Y.; Erlebacher, J. D.; Wagner, A. J.; Searson, P. C. *J. Electrochem. Soc.* **2003**, *150*, C523−C528.

10.1021/cm052262b CCC: $33.50
Published on Web 02/28/2006

Multilayer ferromagnetic/nonmagnetic (FM/NM) nanowires exhibit novel properties, such as giant magnetoresistance, as a result of the interlayer coupling between the ferromagnetic segments. In multilayer nanowires, the current is perpendicular to the plane of the layers, providing a unique geometry for the study of such effects as compared to multilayer thin films where the current is in the plane of the layers. The ability to control the size and aspect ratio of ferromagnetic segments in multilayer nanowires allows additional degrees of freedom that have not been widely explored. In this paper, we report on the fabrication of multilayer Cu/Ni nanowires using potential modulated multilayer deposition (PMMD) from a solution containing both Ni^{2+} and Cu^{2+} ions. In multilayer FM/NM multilayers fabricated using PMMD, the ferromagnetic layer is a Cu_xNi_{1-x} alloy. We use thin film deposition to show how the deposition potential influences the composition and microstructure of the ferromagnetic Cu_xNi_{1-x} layer. We then show how the magnetic properties of multilayer nanowires depend on the aspect ratio of the ferromagnetic segment and on dipolar coupling between the ferromagnetic layers through the nonmagnetic layer. PMMD represents a versatile technique to tailor the magnetic response of ferromagnetic nanowires.

Experimental Procedures

Thin films and nanowires were deposited from a solution containing 0.5 M $NiSO_4$ (Sigma-Aldrich, CAS 10101-97-0), 5 mM $CuSO_4$ (Alfa Aesar, CAS 7758-99-8), and 0.6 M HBO_3 (Alfa Aesar, CAS 10043-35-3) (pH = 3.5). Electrochemical experiments were performed under ambient conditions in a three-electrode Teflon cell with a platinum counter electrode and a Ag/AgCl (3 M NaCl) reference electrode. All potentials are reported with respect to the Ag/AgCl reference (U_{eq} = 0.200 V vs SHE).

Thin Cu_xNi_{1-x} films were deposited on silicon (111) wafers with a 200 nm thick (111) textured Au film and a 5 nm Cr adhesion layer at a constant potential in the range of −0.05 to −1.2 V. The deposition charge was fixed at 2.8 C cm^{-2} corresponding to a film thickness of about 1 μm. The deposition efficiency was 0.85−0.90. Cyclic voltammetry was performed from 0.4 to −1.0 V at a scan rate of 10 mV s^{-1}. Reproducible scans were obtained after two to three cycles.

Multilayer Cu/Ni nanowires were deposited in 6 μm thick polycarbonate templates (Osmonics Inc.) with nominal pore diameters of 30 nm (pore density 6×10^8 cm^{-2}), 50 nm (pore density 6×10^8 cm^{-2}), and 100 nm (pore density 3×10^8 cm^{-2}). The average nanowire diameters, determined from TEM images, were about 40, 75, and 140 nm, respectively, slightly larger than the nominal pore diameter. A 100−300 nm thick gold layer was sputtered onto one side of the template at 5 mTorr as a working electrode for deposition. Ni and Cu layers were electrodeposited at −1.0 and −0.16 V, respectively.

The structure and composition of Cu_xNi_{1-x} alloy thin films were determined from X-ray diffraction measurements (Phillips X'Pert PW 3040) with a Cu Kα source. The lower limit of the grain size was estimated from the peak broadening using the Scherrer equation:[29] $B = k\lambda/s \cos\theta$, where B (rad) is the full-width at half-maximum (fwhm) in the 2θ scan, k is a constant (0.94), λ is the X-ray wavelength (0.154056 nm), s is the grain size, and θ is the angle of the diffraction peak (deg). Note that $B^2 = b^2 - \beta^2$, where b is the experimental fwhm and β is the instrumental broadening (0.06°). Film compositions were determined from the position of the (111) peak. In previous work, we have shown that the lattice parameter obtained from the (111) peak is proportional to the composition of the film.[30] Thus, the peak shift is related to the alloy composition through Bragg's Law: $\lambda = 2d \sin\theta$, where d is the interplanar spacing and θ is the diffraction angle.

The composition of the Cu_xNi_{1-x} films was also determined using Auger electron spectroscopy (PHI 610 Scanning Auger Microprobe) from analysis of the characteristic Cu^1 (920 eV) and Ni^3 (716 eV) peaks.[31] Film compositions were obtained from integration of the Auger peaks and calibrated with respect to the pure copper film deposited at −0.05 V.[32]

For transmission electron microscopy characterization, the nanowires were stripped from the template. First, the sputtered gold layer on the polycarbonate template was removed by contact with mercury. The template was then immersed in chloroform to dissolve the polycarbonate and release the nanowires. The nanowires were rinsed sequentially in acetone, ethanol, and deionized water and then stored in ethanol or deionized water. TEM samples were prepared by placing a drop of the nanowire suspension onto a TEM grid (Ted Pella, Carbon Type-B, 400 mesh). Transmission electron microscope images were obtained on a Phillips 420 TEM at 120 kV.

The magnetization hysteresis loops of arrays of multilayer nanowires were measured at 25 K using a Quantum Design MPMS superconductor quantum interference device (SQUID). The measurements were performed on nanowire arrays with the gold layer removed from the template. Samples were about 10 mm^2 corresponding to about 10^5 nanowires. The saturation magnetization was on the order of 10^{-7} emu. The $M-H$ curves were recorded both perpendicular ($H_\perp$) and parallel ($H_{//}$) to the wire axis. A polycarbonate template was used as a reference.

Micromagnetic simulations of ferromagnetic/nonmagnetic multilayer nanowires were performed using the OOMMF software package (NIST). The relevant parameters used for nickel in the simulations were a saturation magnetization, $M_S = 4.9 \times 10^5$ A m^{-1}; an exchange stiffness, $A = 9 \times 10^{-12}$ J m^{-1}; an anisotropy constant, $K_1 = -5.7 \times 10^3$ J m^{-3}; and a damping coefficient = 0.5.

Results and Discussion

Electrodeposition of Cu_xNi_{1-x} Thin Films and Cu/Ni Multilayer Nanowires. Electrodeposition of multilayer thin films from a single solution containing the ions of the two components is achieved by modulation of the potential (or current) and usually results in the deposition of a compositionally modulated multilayer with a bilayer repeat unit of the form A_xB_{1-x}/A_yB_{1-y}.[33−35] For the case where the difference in equilibrium potentials of A and B is sufficiently large (typically > 0.4 V) and the concentration of the more noble component is very low (i.e., $[A^{n+}] \ll [B^{m+}]$), multilayers of

(29) Jenkins, R.; Snyder, R. L. *Introduction to X-ray powder Diffractometry*; Wiley: New York, 1996.
(30) Sun, L.; Chien, C. L.; Searson, P. C. *Chem. Mater.* **2004**, *16*, 3125−3129.
(31) Chastain, J. C.; King, R. C. *Handbook of Photoelectron Spectroscopy*; Physical Electronics: Eden Prairie, MN, 1995.
(32) Czanderna, A. W. *Methods of surface analysis*; Elsevier Scientific Pub. Co.: Amsterdam, 1975.
(33) Yahalom, J.; Zadok, O. *J. Mater. Sci.* **1987**, *22*, 499−503.
(34) Lashmore, D. S.; Dariel, M. P. *J. Electrochem. Soc.* **1988**, *135*, 1218−1221.
(35) Tench, D. M.; White, J. T. *J. Electrochem. Soc.* **1990**, *137*, 3061−3066.

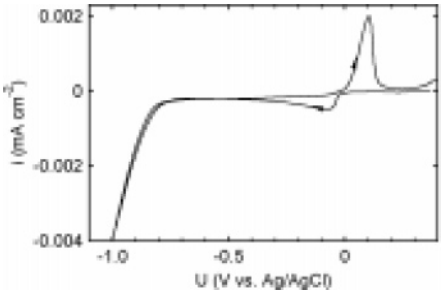

Figure 1. Cyclic voltammogram for gold in 0.5 M $NiSO_4$, 0.005 M $CuSO_4$, and 0.6 M HBO_3 at a scan rate of 10 mV s^{-1}.

the form A_xB_{1-x}/A can be deposited. In this case, A (e.g., Cu) is deposited at more positive potentials, and an A_xB_{1-x} alloy (e.g., Cu_xNi_{1-x}) is deposited at more negative potentials.

Although we focus here on the deposition of Cu/Ni multilayer nanowires from solution containing both Cu(II) and Ni(II) ions, it is important to determine the properties of the ferromagnetic Cu_xNi_{1-x} layer. Thus, we first describe results of experiments on thin films to determine the influence of deposition potential on the film composition and microstructure.

Figure 1 shows a cyclic voltammogram for gold in 0.5 M $NiSO_4$, 0.005 M $CuSO_4$, and 0.6 M H_3BO_3. On scanning the potential negative from the open circuit potential, the current onset at about +0.05 V is followed by a small peak associated with the nucleation and growth of copper. The current onset for copper deposition is close to the equilibrium potential for the Cu^{2+}/Cu couple in this solution $U_{eq}(Cu^{2+}/Cu) = 0.072$ V. Due to the low Cu^{2+} concentration, the deposition is diffusion-limited over a wide potential range from about −0.15 V to the onset of nickel deposition at about −0.7 V. The equilibrium potential for the Ni^{2+}/Ni couple in this solution is $U_{eq}(Ni^{2+}/Ni) = -0.468$ V, indicating a nucleation overpotential of about 0.23 V. On the reverse scan, there is little hysteresis in the nickel deposition region, and the diffusion-limited deposition of copper is seen up to about 0 V. The single oxidation peak is associated with the stripping of copper; nickel dissolution is negligible in this solution.[35] The electrochemical etching of copper from Cu_xNi_{1-x} alloys has been exploited in the synthesis of nanoporous nickel films.[30]

X-ray diffraction patterns for Cu_xNi_{1-x} films show a strong (111) texture with no evidence of other peaks. Figure 2a shows diffraction patterns for films deposited at potentials from −0.05 to −1.20 V. At the most positive deposition potential, −0.05 V, the (111) peak is close to the value of 43.297° for pure Cu. With increasing deposition potentials, the (111) peak shifts toward the value of 44.507° characteristic of pure Ni. The single (111) peak at all deposition potentials illustrates that the films are a single phase solid solution of nickel and copper. The grain size, determined from the full width at half-maximum of the (111) peak, is shown in Figure 2b. The grain size is about 30 nm at all deposition potentials.

Figure 3 shows the dependence of the film composition on the deposition potential. The mole fraction of Cu is close to 1.0 at potentials positive to the equilibrium potential for Ni. At more negative potentials, the mole fraction of Cu

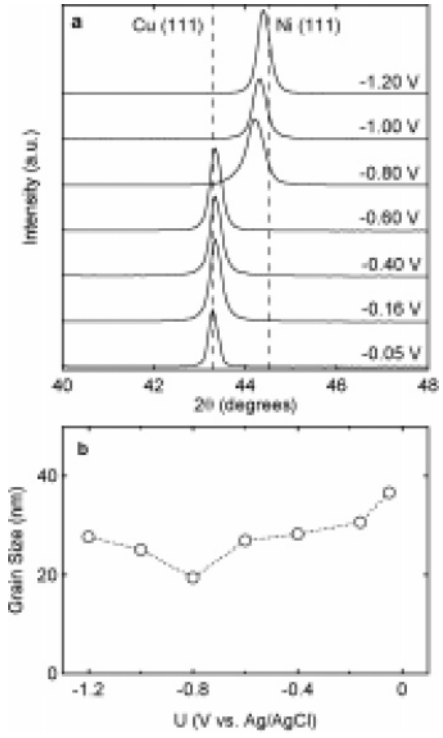

Figure 2. (a) X-ray diffraction patterns for Cu_xNi_{1-x} thin films as a function of deposition potential. The dashed lines correspond to the Ni (111) and Cu (111) peaks at 44.507 and 43.297°, respectively. (b) Grain size vs the deposition potential.

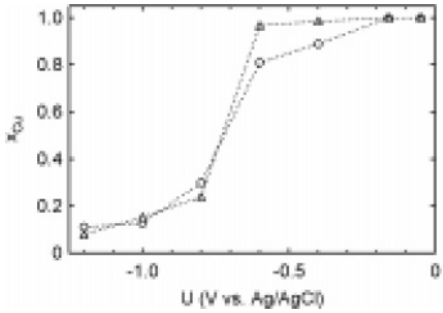

Figure 3. Dependence of film composition on deposition potential, (○) Auger electron spectroscopy and (△) X-ray diffraction. Cu_xNi_{1-x} thin films were deposited from 0.5 M $NiSO_4$, 0.005 M $CuSO_4$, and 0.6 M HBO_3.

decreases rapidly to a value of about 0.10. At −1.0 V, where we deposit the Ni-rich segments of the multilayer nanowires, the mole fraction of Cu is about 0.12. Since the magnetization of Cu_xNi_{1-x} alloys decreases with increasing copper concentration, it is desirable to minimize the mole fraction of copper in the ferromagnetic segments. This can be achieved by depositing at more negative potentials, as can be seen from Figure 3; however, this must be balanced by the increase in hydrogen evolution kinetics that results in poor interface quality. By comparison, the Ni-rich layer in Cu/Ni multilayers deposited at a constant current from a single bath containing 0.3 M $NiSO_4$ and 0.041 M $CuSO_4$ was $Cu_{0.19}Ni_{0.81}$.[36]

To ensure reproducible layer thickness in multilayer nanowires, the deposition charge rather than the time for deposition is controlled. The layer thickness for a segment

(36) Toth-Kadar, E.; Peter, L.; Becsei, T.; Toth, J.; Pogany, L.; Tarnoczi, T.; Kamasa, P.; Bakonyi, I.; Lang, G.; Cziraki, A.; Schwarzacher, W. *J. Electrochem. Soc.* **2000**, *147*, 3311−3318.

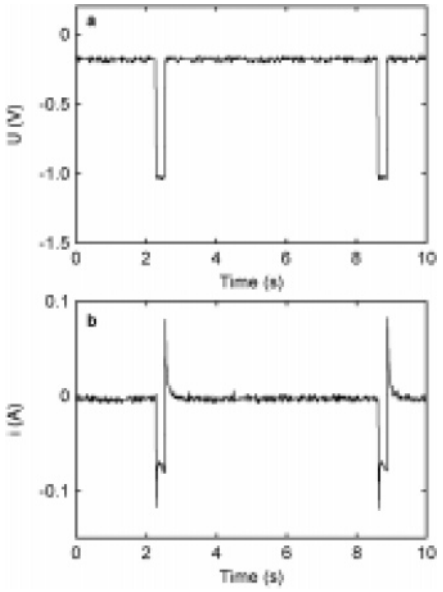

Figure 4. (a) Applied potential vs time and (b) current vs time transient for the deposition of $[Ni(5\ nm)/Cu(5\ nm)]_{250}$ multilayer nanowires in a polycarbonate template with a pore diameter of 50 nm and pore density of $6 \times 10^8\ cm^{-2}$.

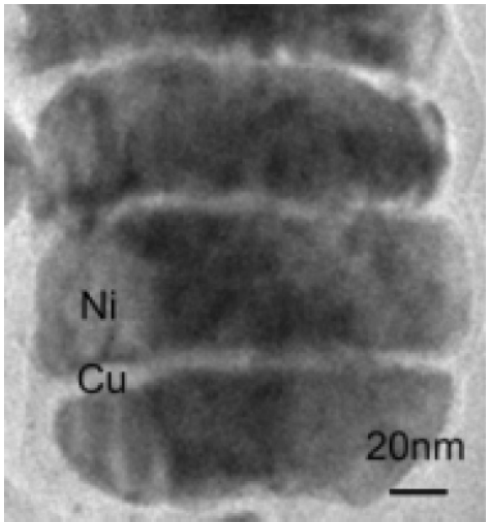

Figure 5. Transmission electron microscope image of a 140 nm diameter nanowire with 40 nm Ni layers and 5 nm Cu layers.

is given by $t = \eta Q V_m / nFA$, where η is the deposition efficiency, Q is the charge passed, V_m is the molar volume of the component, F is Faraday's constant, and A is the total area of the pores. The potential was switched when the charge reached a value corresponding to the required layer thickness. Multilayers were deposited by switching between -0.16 and -1.0 V. Figure 4a shows a typical applied potential waveform, and Figure 4b shows the corresponding current response for deposition of multilayer nanowires with 5 nm Cu and 5 nm Ni. Since the Ni(II) concentration is relatively high (0.5 M), the current associated with nickel deposition at -1 V is relatively large, and the 5 nm nickel layers are deposited in about 0.25 s. In contrast, the Cu(II) concentration is much lower (5 mM), and the copper deposition current is much lower; hence, 5 nm copper layers are deposited in about 6 s.

Figure 5 shows a bright field transmission electron microscope image of a Cu/Ni multilayer nanowire with 40 nm Ni segments (dark regions) and 5 nm Cu segments (bright regions). This image illustrates the reproducible multilayer structure, sharp interfaces, and nanoscale layer thicknesses that can be achieved with electrodeposition. Note that the nickel segments contain a small amount of copper due to the co-deposition of copper (see Figure 3).

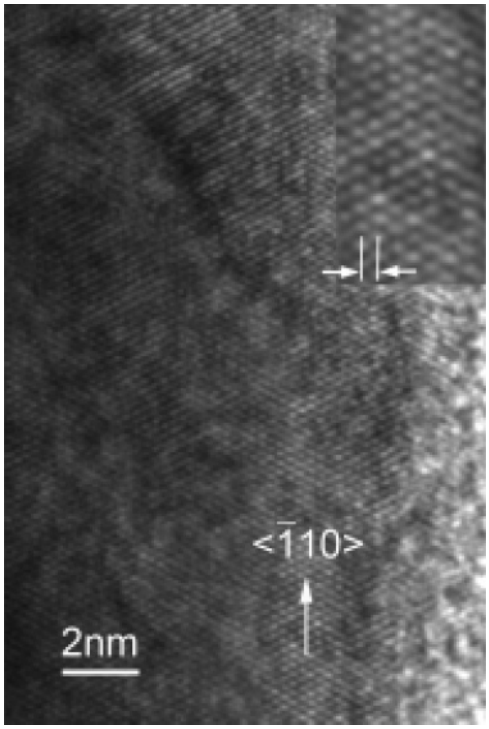

Figure 6. High-resolution TEM image of a Ni segment in a 100 nm diameter multilayer nanowire with 10 nm Ni layers and 5 nm Cu layers. The growth direction is the $\langle\bar{1}10\rangle$ direction. The inset shows part of the image at high magnification.

Figure 6 shows a high-resolution transmission electron microscope image of a portion of a Ni-rich segment in a multilayer nanowire. As shown in Figure 2, electrodeposited Cu_xNi_{1-x} films have a preferred growth direction along the $\langle 111\rangle$ direction;, however, the nickel nanowire segments exhibit a preferred $\langle\bar{1}10\rangle$ growth direction. The inset shows a region with a well-defined (111) plane. From the interplanar spacing, we estimate a lattice parameter of 3.53 Å, which corresponds to a Cu_xNi_{1-x} alloy ($a_{Ni} = 3.524$ Å and $a_{Cu} = 3.615$ Å) with $x_{Cu} \approx 0.07$, slightly lower than the value of 0.12 obtained for thin films from Auger electron spectroscopy.

Dubois et al.[24] reported on the deposition of 90 nm diameter Cu/NiFe nanowires in polycarbonate templates from a single sulfate bath. TEM analysis of the nanowires revealed a $\langle\bar{1}10\rangle$ growth direction for the NiFe layers along the wire axis. Wang et al.[22] reported on the deposition of 70 nm diameter Cu/Ni multilayer nanowires from 2 M nickel sulfamate and 0.02 M copper sulfate (pH = 3.5−4.0) into polycarbonate templates. The preferred growth direction for the Ni segments was along the $\langle 111\rangle$ direction. Although these results suggest that the preferred $\langle\bar{1}10\rangle$ growth direction is associated with the sulfate solution, the pore diameter and deposition potential also influence the microstructure.

A common feature of the microstructure of multilayer nanowires electrodeposited in porous templates is stacking faults.[26] Figure 7 shows a high-resolution transmission

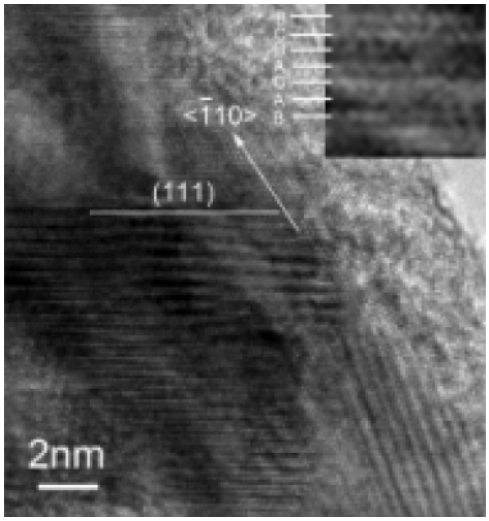

Figure 7. High-resolution TEM image of a Ni segment in a 100 nm diameter multilayer nanowire with 10 nm Ni layers and 5 nm Cu layers showing a high density of twins. The inset shows the stacking of adjacent {111} planes.

electron microscope image of the Ni-rich segment of a Ni/Cu multilayer nanowire. In this segment, a series of fcc {111} twins are seen adjacent to a twin-free single crystal. The segment is oriented such that the (111) plane can be clearly seen. As described previously, growth occurs preferentially along the $\langle\bar{1}10\rangle$ direction. The fcc stacking twin structure can be clearly distinguished in the inset. We note that strong twinning has been reported for nickel films deposited from sulfamate solution on Cu (110) and Cu (111).[37]

Magnetic Properties of Cu/Ni Multilayer Nanowires. Ferromagnetic nanowires exhibit unique and tunable magnetic properties due to the inherent shape anisotropy and the small wire dimensions. In fcc Ni, the magnetic easy axis is along the [111] direction, and the magnetic hard axis is along the [100] direction. However, the magnetocrystalline anisotropy for nickel is relatively small with an anisotropy energy constant of $K_1 = -4.5 \times 10^4$ erg cm^{-3}, about an order of magnitude lower than for Fe and 2 orders of magnitude lower than for Co.[38] As a result, the magnetic response is dominated by the shape and aspect ratio of the nickel segments. Also, from the pore density in the polycarbonate membranes, the average spacing between the nanowires is 350−400 nm. These dimensions are sufficiently large that wire−wire interactions can be neglected.[9]

The transition between multidomain and single domain structures is dependent on diameter and aspect ratio. Nickel nanowires with an aspect ratio of 10 would be expected to be single domain for diameters less than about 600 nm.[38] For an aspect ratio of 2, the critical diameter decreases to about 150 nm. Thus, most of the nickel segments in this study are expected to be single domain.

Figure 8 shows M−H curves for Cu/Ni multilayer nanowires where the ferromagnetic Ni segments have aspect ratio of 2.5 (rod-shaped), 1.0 (intermediate), and 0.1 (disk-shaped), respectively. Figure 8a shows magnetization curves for 50

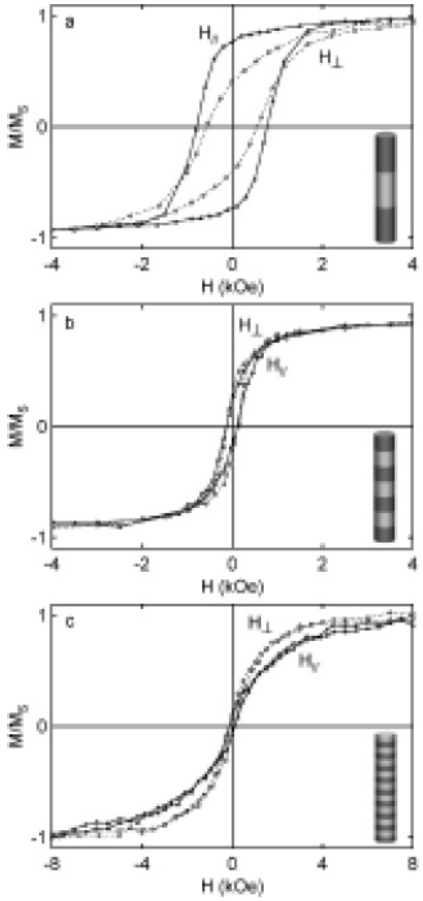

Figure 8. Magnetic hysteresis loops of electrodeposited Cu/Ni multilayer nanowires embedded in polycarbonate templates. (a) [Ni(125 nm)/Cu(125 nm)]$_{10}$, d = 50 nm (rod-shaped Ni segments; aspect ratio = 2.5); (b) [Ni(100 nm)/Cu(100 nm)]$_{30}$, d = 100 nm (intermediate-shaped Ni segments; aspect ratio = 1.0); and (c) [Ni(5 nm)/Cu(5 nm)]$_{250}$, d = 50 nm (disk-shaped Ni segments; aspect ratio = 0.1).

Table 1. Summary of Magnetic Properties of Multilayer Nanowires

	[Ni(125 nm)/ Cu(125 nm)]$_{10}$	[Ni(100 nm)/ Cu(100 nm)]$_{30}$	[Ni(5 nm)/ Cu(5 nm)]$_{250}$
d (nm)	50	100	50
FM aspect ratio	2.5	1.0	0.1
H_C (//) (Oe)	790	128	120
H_C (⊥) *(Oe)*	570	122	106
M_r/M_s (//)	0.77	0.22	0.09
M_r/M_s (⊥)	0.43	0.31	0.07

nm diameter [Ni(125 nm)/Cu(125 nm)]$_{10}$ multilayer nanowires where the ferromagnetic Ni segments have an aspect ratio of 2.5. The easy axis is parallel to the wire axis, as can be seen from the large remanence (M/M_s = 0.774) and coercivity (H_C = 790 Oe). Perpendicular to the wire axis, the magnetization curves are characterized by small remanence (0.432) and coercivity (570 Oe) and a large saturation field (≈4500 Oe). The results are summarized in Table 1.

Figure 8b shows M−H curves for 100 nm diameter [Ni(100 nm)/Cu(100 nm)]$_{30}$ multilayer nanowires. In this case, the aspect ratio of the Ni segments is 1.0. The magnetization curves are essentially identical with the applied field perpendicular or parallel to the wire axis. In both cases, the coercivity and remanence are very small, and the saturation field is relatively large. Similar features have been reported for Ni cylinders with an aspect ratio close to 1.0;[1] however, the coercivity and remanence are smaller for the

(37) Verma, S. K.; Wilman, H. *J. Phys. D: Appl. Phys.***1971**, *4*, 1167−1175.
(38) O'Handley, R. C. *Modern magnetic materials: principles and applications*; Wiley: New York, 2000.

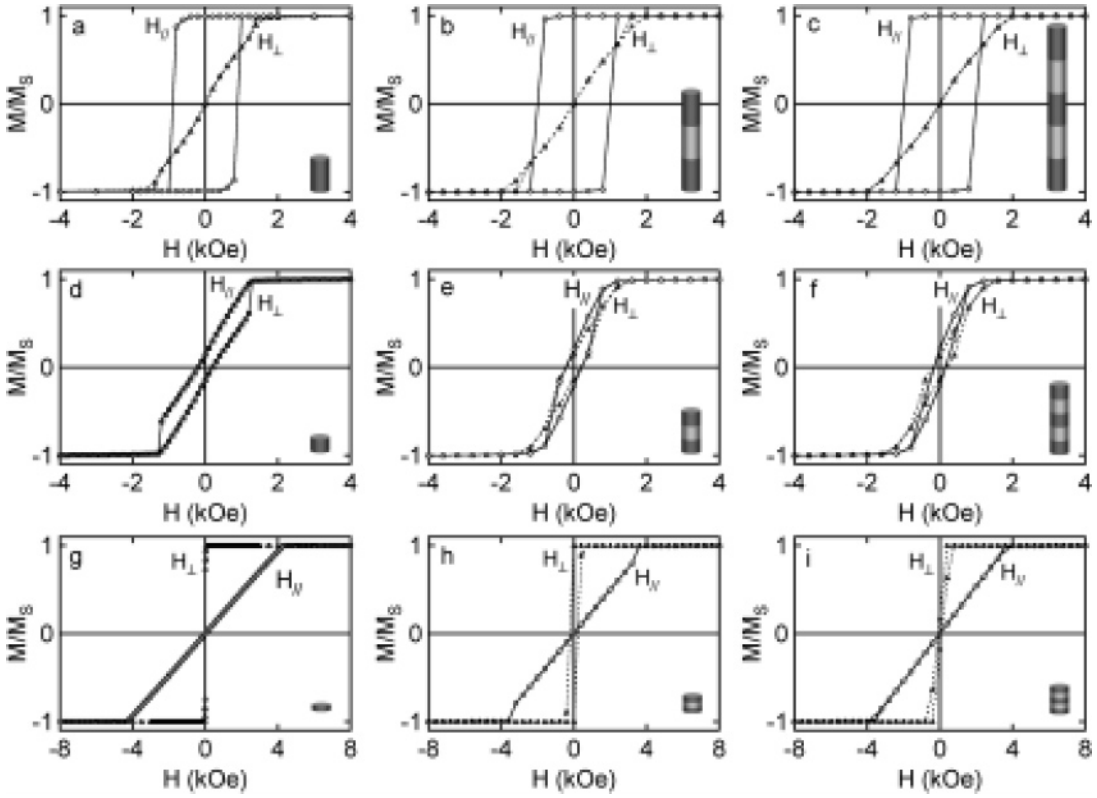

Figure 9. Micromagnetic simulations of structures with one, two, and three ferromagnetic nickel segments. (a) A single rod-shaped Ni segment, $d = 50$ nm, $l = 125$ nm; (b) Ni(125 nm)/Cu(125 nm)/Ni(125 nm), $d = 50$ nm; (c) Ni(125 nm)/Cu(125 nm)/Ni(125 nm)/Cu(125 nm)/Ni(125 nm), $d = 50$ nm; (d) a single intermediate-shaped Ni segment, $d = 100$ nm, $l = 100$ nm; (e) Ni(100 nm)/Cu(100 nm)/Ni(100 nm), $d = 100$ nm; (f) Ni(100 nm)/Cu(100 nm)/Ni(100 nm)/Cu(100 nm)/Ni(100 nm), $d = 100$ nm; (g) a single disk-shaped Ni segment, $d = 50$ nm, $l = 5$ nm; (h) Ni(5 nm)/Cu(5 nm)/Ni(5 nm), $d = 50$ nm; and (i) Ni(5 nm)/Cu(5 nm)/Ni(5 nm)/Cu(5 nm)/Ni(5 nm), $d = 50$ nm.

multilayer nanowires. The demagnetization factors (H_s/M_s) in both directions are close to the value of $4\pi/3$ ($H_s = 2030$ Oe) for a sphere, consistent with a cylinder of aspect ratio 1.0.

Figure 8c shows M−H curves for 50 nm diameter $[Ni(5\ nm)/Cu(5\ nm)]_{250}$ multilayer nanowires. In this case, with disk-shaped Ni segments, the easy axis is perpendicular to the wire axis. In both perpendicular and parallel orientations, the remanence (0.07−0.09) and coercivity (106−120 Oe) are small. The very small remanence along the easy axis is related to dipolar coupling between adjacent ferromagnetic segments when the separation between them is sufficiently small. This effect is particularly important for applications involving magnetic particles in suspension since the very low remanence minimizes magnetic aggregation of particles, although they can exhibit a relatively large magnetic moment.

Figure 9 shows micromagnetic simulations of single nickel segments and multisegment structures with one, two, or three ferromagnetic segments. The dimensions are the same as for the experimental measurements described previously. Figure 9a−c shows M−H loops for structures with one, two, and three 50 nm diameter rod-shaped Ni segments (aspect ratio = 2.5). The curves exhibit the expected square loop parallel to the axial direction and a sheared loop with negligible coercivity perpendicular to the axial direction. Dipolar coupling between the ferromagnetic segments favors head-to-tail alignment of the magnetic moments along the nanowire axis but is expected to be relatively weak due to the relatively large spacing (125 nm). Comparison of the curves shows that dipolar coupling between segments results in a small increase in coercivity along the easy axis, a small increase in the remanence, and a small increase in the saturation field along the hard axis. While these curves capture some of the features of the experimental results shown in Figure 8a, there are clearly significant differences.

Figure 9d−f shows the M−H loops for structures with one, two, and three 100 nm diameter intermediate-shaped Ni segments (aspect ratio = 1.0). The M−H loops are similar both parallel and perpendicular to the axial directions, and the influence of dipolar coupling is relatively weak. In this case, the simulations with multiple nickel segments capture the key features of the experimental results.

Figure 9g−i shows M−H loops for structures with one, two, and three 50 nm diameter disk-shaped Ni segments (aspect ratio = 0.1). The M−H loops show that the easy axis is perpendicular to the axial direction. Dipolar interactions between the ferromagnetic segments favor anitparallel alignment of the magnetic moments perpendicular to the nanowire axis. With the small nonmagnetic layer thickness (5 nm), dipolar interactions are significant, resulting in a decrease in squareness (M_r/M_s) from 1.0 to almost zero with three ferromagnetic layers. While the simulations with three nickel segments capture the general features of the experiments, in particular, the dramatic decrease in remanence, the M−H loops obtained from experiments are noticeably more sheared.

A feature of the polycarbonate templates is that the pores exhibit an angular spread of up to 30°. This distribution would be expected to influence the magnetic response for nanowires with ferromagnetic segments larger than or smaller

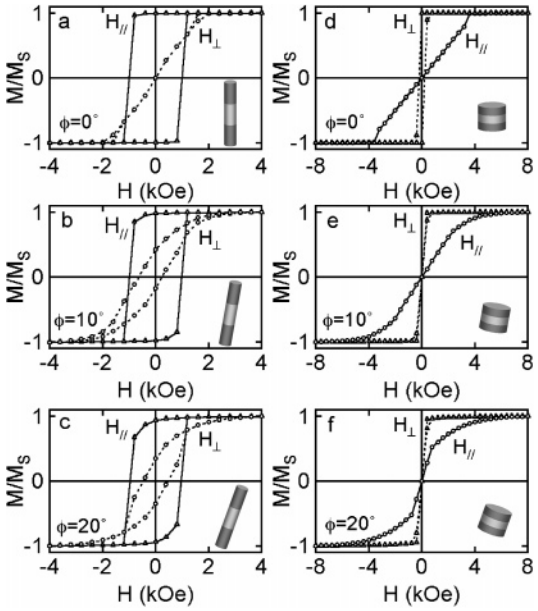

Figure 10. Micromagnetic simulations of 50 nm diameter Ni/Cu/Ni structures, (a−c) Ni(125 nm)/Cu(125 nm)/Ni(125 nm) with tilt angles of 0, 10, and 20°, respectively; and (d−f) Ni(5 nm)/Cu(5 nm)/Ni(5 nm) structures with tilt angles of 0, 10, and 20°, respectively.

than 1.0 where shape anisotropy is important. Figure 10 shows simulations for 50 nm diameter Ni/Cu/Ni structures where the segments have aspect ratios of 2.5 and 0.1, respectively, and the structures are tilted at angles of 0, 10, and 20° with respect to the applied magnetic field. Figure 10a−c shows M−H loops for the rod-shaped nickel segments. Increasing the tilt angle results in a small decrease in the remanence along the easy axis but a large increase in coercivity along the hard axis. The simulations with a 10−20° tilt show good agreement with the experimental results.

Figure 10d−f shows the corresponding dependence of the M−H loops for the disk-shaped nickel segments. Increasing the tilt angle results in shearing of the loops both parallel and perpendicular to the axial direction. The simulations with 10−20° tilt show very good agreement with the experimental results. The small differences can be attributed to effects related to the nonuniformities in the layer thickness (5 nm).

Conclusion

Electrodeposition has been used to fabricate Cu/Ni multilayer nanowires. Magnetic measurements show that the magnetic properties such as the magnetic easy axis, coercivity, remanence, and saturation field can be tailored by engineering the nanowires with a different composition, aspect ratio, diameter, and spacing of ferromagnetic layers.

Acknowledgment. This work was supported by the JHU MRSEC (NSF Grant DMR05-20491).

CM052262B